Title	Deep-level defects in n-type 6H silicon carbide induced by He implantation
Author(s)	Ling, CC; Chen, XD; Brauer, G; Anwand, W; Skorupa, W; Wang, HY; Weng, HM
Citation	Journal Of Applied Physics, 2005, v. 98 n. 4
Issued Date	2005
URL	http://hdl.handle.net/10722/146196
Rights	Journal of Applied Physics. Copyright © American Institute of Physics.

Deep-level defects in n-type 6H silicon carbide induced by He implantation

C. C. Ling, X. D. Chen, G. Brauer, W. Anwand, W. Skorupa et al.

Citation: J. Appl. Phys. **98**, 043508 (2005); doi: 10.1063/1.2014934
View online: http://dx.doi.org/10.1063/1.2014934
View Table of Contents: http://jap.aip.org/resource/1/JAPIAU/v98/i4
Published by the American Institute of Physics.

Deep-level defects in *n*-type 6H silicon carbide induced by He implantation

C. C. Ling[a] and X. D. Chen
Department of Physics, The University of Hong Kong, Pokfulam Road, Hong Kong, People's Republic of China

G. Brauer, W. Anwand, and W. Skorupa
Institut für Ionenstrahlphysik und Materialforschung, Forschungszentrum Rossendorf, Postfach 510119, D-01314 Dresden, Germany

H. Y. Wang
Department of Physics, The University of Hong Kong, Pokfulam Road, Hong Kong, People's Republic of China and Department of Modern Physics, University of Science and Technology of China, Hefei 230026, People's Republic of China

H. M. Weng
Department of Modern Physics, University of Science and Technology of China, Hefei 230026, People's Republic of China

(Received 21 January 2005; accepted 11 July 2005; published online 18 August 2005)

Defects in He-implanted *n*-type 6H–SiC samples have been studied with deep-level transient spectroscopy. A deep-level defect was identified by an intensity with a logarithmical dependence on the filling pulse width, which is characteristic of dislocation defects. Combined with information extracted from positron-annihilation spectroscopic measurements, this defect was associated with the defect vacancy bound to a dislocation. Defect levels at 0.38/0.44 eV (E_1/E_2), 0.50, 0.53, and 0.64/0.75 eV (Z_1/Z_2) were also induced by He implantation. Annealing studies on these samples were also performed and the results were compared with those obtained from e^--irradiated (0.3 and 1.7 MeV) and neutron-irradiated *n*-type 6H–SiC samples. The E_1/E_2 and the Z_1/Z_2 signals found in the He-implanted sample are more thermally stable than those found in the electron-irradiated or the neutron-irradiated samples. © *2005 American Institute of Physics*. [DOI: 10.1063/1.2014934]

I. INTRODUCTION

Silicon carbide is a wide-band-gap semiconductor suitable for fabricating high-temperature, high-power, and high-frequency electronic devices.[1] As the knowledge of defects in the material is crucial for successful device fabrication, defects in SiC have been extensively studied by various experimental methods such as deep-level transient spectroscopy (DLTS).[2–18] DLTS is a very useful technique for characterizing the deep-level defects and it has been employed to study deep levels in *n*-type 6H–SiC induced by electron irradiation, neutron irradiation, proton irradiation, and ion implantation. Deep-level defects such as 0.23 eV (ED1), 0.36/0.44 eV (E_1/E_2), 0.43–0.46 eV (RD5), 0.50 eV (E_i), and 0.62/0.68 eV (Z_1/Z_2) have been identified below the conduction band.[2–18] Despite a great deal of effort devoted to understanding these deep-level defects, knowledge of these defects is far from complete and remains controversial.

As reported from different research groups, the type of defects created and their subsequent annealing properties were found to vary from case to case, being dependent on the type of irradiating particles and also on the particle energy. For example, the Z_1/Z_2 in He-implanted 6H–SiC have been reported to be thermally stable at 1700 °C,[2,4] and in some other studies of electron-irradiated 6H–SiC, they annealed at a relatively low temperature of 900 °C.[6,7] A discrepancy has also been found in the case of E_1/E_2, in which the annealing temperature has been reported to be 1400 °C (Ref. 9) and higher than 1700 °C.[4] However, it is also worth mentioning that the discrepancy can also be due to the different starting SiC material and different sample pre- or postirradiation treatments. These uncertainties led us to conduct a series of systematic studies of the deep-level defects in a similar *n*-type 6H–SiC starting material induced by different particle irradiations and also to study their annealing behaviors under similar annealing treatments and measuring processes. We have already reported the DLTS studies performed on electron- and neutron-irradiated *n*-type 6H–SiC samples.[6,12,13] In the as-neutron-irradiated sample, Z_1/Z_2 are the most intense peaks while other signals such as ED1, E_1/E_2, and E_i (or RD5) also exist.[12] The E_1/E_2 signals grow with increasing annealing temperature and after the 900 °C annealing, they are the only remaining signals. These E_1/E_2 peaks finally anneal after the 1400 °C annealing. For electron energy $E_e < 0.3$ MeV, no DLTS signal was found after the irradiation.[13] For irradiation with electrons having energies just above the atomic displacement threshold (i.e., $E_e = 0.3$ MeV), the most intense DLTS signals are E_1/E_2, while ED1 and E_i are observed as well.[13] For samples irradiated with high-energy electrons (i.e., 1.7 MeV), Z_1/Z_2 and a defect with an activation energy of $E_C - 0.31$ eV were also created.[6,16] The 0.31-eV deep-level peak overlaps with the E_1/E_2 peaks.

In the present study, with the use of the DLTS technique,

[a]Author to whom correspondence should be addressed; electronic mail: ccling@hku.hk

we have studied the deep-level defects in *n*-type 6H–SiC samples induced by He implantation. The annealing behaviors of these induced defects were also investigated. The properties of the defects found in the present He-implanted samples are compared with those induced by the 0.3-MeV electron irradiation, the 1.7-MeV electron irradiation, and the neutron irradiation. In these studies, all the samples were cut from the wafers manufactured under the same environment and had the same sample treatment and measurement processes.

II. EXPERIMENT

As in our previous studies,[11–13,16] the starting material used in the present study was 5-μm-thick nitrogen-doped (0001)-oriented epilayer ($n=1\times10^{16}$ cm^{-3}) grown on $n^+-6H-SiC$ substrate ($n=8\times10^{17}$ cm^{-3}) purchased from Cree Research Inc. Ohmic contacts were fabricated on the side of the n^+ substrate. He implantation was performed with ion energies of 55, 210, 430, 665, and 840 keV (each with fluence of 2×10^{11} cm^{-2}) so as to produce a box-shaped implanted layer with a depth of ~2 μm. He implantation was carried out onto the epi side of the samples. We have also performed He implantation with higher dosages on the samples and found the resulting as-implanted samples were not suitable for DLTS measurement because of the high resistivity. After the irradiation processes, Schottky contacts were then made on the epi side by evaporating 0.6-mm-diameter Au dots. The quality of all the samples was ensured by performing *I-V* and *C-V* measurements. Each of the annealing steps involved annealing the sample in a flowing Ar atmosphere for 30 min. Unless specified, the DLTS measurements were performed with the reverse bias, the filling pulse width, and the rate window width being equal to 16 V, 1 ms, and 6.82 ms, respectively. The ionization energies and the capture cross sections of the identified defects were found conventionally by the Arrhenius plots.

III. RESULTS AND DISCUSSIONS

The DLTS spectra of the He-implanted sample annealed at different temperatures are shown in Figs. 1(a) and 1(b). Some major signals, namely, at temperatures of 170–240, $\sim$250 and the broad signal at 300–380 K were observed in these He-implanted spectra. We have also measured the DLTS spectrum of the as-grown *n*-type 6H–SiC sample and no defect signal was observed (with DLTS limiting $\sim10^{12}$ cm^{-3}). This implies all these DLTS peaks were generated by the He-implantation process.

A. Broad signal at $T=300-380$ K

1. Peak at $T=325$ K in samples with annealing temperatures below 500 °C: Dislocation-related defect

A broad signal appeared in the as-implanted sample at $T=300-380$ K and from the figure this broad signal seems to consist of at least two peaks, namely, one at $\sim$325 K and another at $\sim$350 K. After applying the bias to the sample to measure the DLTS spectrum, the 350-K peak disappeared under further measurement [as shown in Fig. 1(a)]. It is also worth mentioning that the present 350-K peak was not found

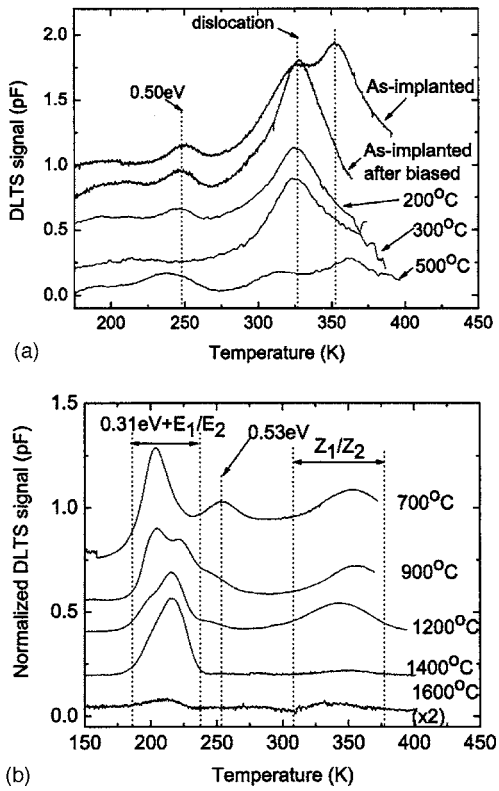

FIG. 1. DLTS spectra of the He-implanted *n*-type 6H silicon carbide samples annealed at different temperatures. These spectra were taken with reverse bias, filling pulse width, and rate window width equal to −16 V, 1 ms, and 6.82 ms, respectively.

in the first measured DLTS spectrum if the He-implanted sample was preannealed at 200 °C. These observations seem to suggest that the 350-K peak anneals at temperatures below the maximum temperature of the DLTS measurement (i.e., 400 K).

It is interesting to notice that the activation energy of the 325-K peak is dependent on the reverse bias applied in the DLTS measurement. As shown in the Arrhenius plot of Fig. 2, the activation energy varies from 0.89 to 0.61 eV as the reverse bias changes from −16 to −2 V, for which a constant value of activation energy would be expected for a common deep-level point defect. Another interesting prop-

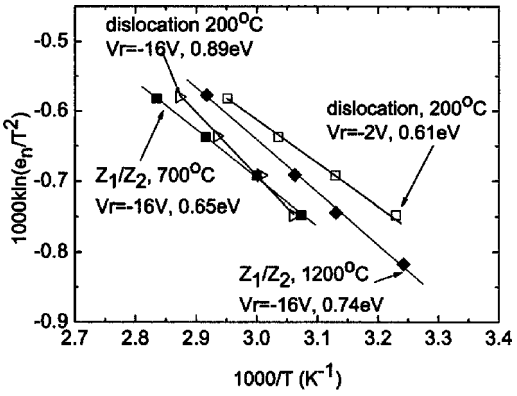

FIG. 2. Arrhenius plots of the dislocation-related defects taken with $V_r=-16$ and −2 V from the 200 °C annealed sample, and those of the Z_1/Z_2 signals taken from the 700 and 1200 °C annealed samples. All of these signals are in the temperature range of 300–380 K.

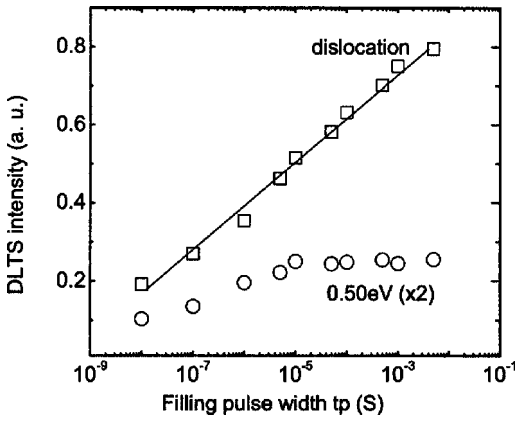

FIG. 3. DLTS intensities of the dislocation defect and the 0.50-eV deep levels as a function of the filling pulse width (t_p).

erty is the carrier-capture dynamic of this defect. Figure 3 shows the intensity of this peak as a function of the filling pulse width t_p. It is clearly shown that the peak intensity of this defect grows logarithmically with t_p for a wide range of t_p (from 10^{-8} to $\sim 10^{-2}$ s). For most deep-level point defects, the electron-capture process in the trap-filling period is described by the rate equation $dN_f/dt = n\nu\sigma(N_{\text{total}} - N_f)$, where N_f is the concentration of the deep level filled with electron, n is the free-electron density, ν is the free-electron thermal velocity, σ is the electron-capture cross section, and N_{total} is the total concentration of the deep level. The filled electron trap density after applying the filling pulse for a period of t_p can thus be found by solving the rate equation and the result is given by $N_f(t_p) = N_{\text{total}}(1 - \exp[-n\nu\sigma t_p])$. This implies that the N_f and thus also the DLTS intensity saturate with t_p in an exponential way. This is best illustrated by the t_p dependence of the neighboring peak at $\sim$250 K, as shown in Fig. 3.

The logarithmic capture rate dependence on t_p is a characteristic behavior for a free carrier trapped along a line dislocation.[19–22] A model involving a barrier-limited capture rate has been derived and has been used to describe the electron-capture process due to extended line defects, in which the trapped electron resided along the line.[19,20] In this model, the electrons already trapped by the defect present a Coulombic barrier $\Phi(t)$ for trapping further electrons. The concentration of free electrons that have sufficient energy to overcome the barrier is given by $n\exp(-q\Phi(t)/kT)$. The rate equation for electron capture is thus given by $dN_f/dt = n\nu\sigma_n(N_T - N_f)\exp(-q\Phi(t)/kT)$. The solution of this rate equation describes the filling pulse period dependence of the filled trap states density, i.e., $N_f(t) = n\nu\sigma_n\tau N_T \ln(t_p/\tau)$. τ is the time constant given by $\tau = (kT/q\Phi_{\text{eq}})(N_{f,\text{eq}}/N_T)(1/\sigma_n\nu n)$, where Φ_{eq} and $N_{f,\text{eq}}$ are the Coulombic barrier height and the filled trap density at equilibrium, respectively. We thus suggest that the 325-K peak defect is an extended line defect, which is possibly a dislocation. Dislocation defects exhibiting similar logarithmic peak dependence on t_p have also been reported in plastically deformed semiconductors [e.g., Si (Ref. 19) and GaAs (Ref. 20)], He-implanted GaN,[21] Ni/6H–SiC Schottky diodes,[22] and proton-irradiated 4H–SiC.[17] It is also worth to point out that the apparent activation energy extracted from the Arrhenius plot (for example, those shown in Fig. 2) is indeed the average energy of the filled defect state weighted by the density-of-states distribution, rather than the exact energy required for the carrier to be emitted from the deep level as in the common point defect deep-level picture. From Fig. 1(a), it is also noticed that this 325-K peak signal is significantly weakened by the 500 °C annealing. Dislocation defects in SiC have also been identified and investigated with other methods such as observing the chemically etched pits.[23–26]

With the aim of extracting further information relating to this defect, we have performed positron-annihilation spectroscopic (PAS) measurements on the samples using a variable-energy positron beam.[27–31] PAS is a very useful technique in investigating open-volume defects in semiconductors.[27–29] Positrons implanted into the samples rapidly thermalize and then undergo diffusion. Negatively charged or neutral open-volume defects present a potential well to the diffusing positrons that can trap them into localized defect bound states. The working principle of PAS is that the outgoing 511-keV annihilation gamma photons carry information on the electronic environment at which the positrons annihilate. In the present measurements, the Doppler broadening of the annihilation gamma photon was measured. As the positron is trapped in the open-volume defect, more annihilation events originate from valence electrons relative to core electrons. Because of the relatively lower momentum of valence electrons, positron trapping in open-volume defects results in a less Doppler-broadened annihilation spectrum. The Doppler broadening is usually parametrized by the S parameter, which is a measure of the fraction of positrons annihilating with valence electrons. A higher S-parameter value implies more positrons annihilating at the open-volume defect site. Moreover, the measured positron diffusion length L_+ also yields useful information. A decrease in L_+ is also a good indication of positrons getting trapped by defect centers.

We have performed S-parameter measurements on the samples with different positron incident energies so as to obtain the S-parameter depth profile of the sample system. Using the program VEPFIT,[32] we have fitted our data by a model consisting of a box-shaped defective layer induced by He implantation and the nondefective SiC bulk. In the model, positrons implanting into and diffusing in the solid get trapped by different open-volume defects and annihilate at various states. The S parameter and the L_+ of the defective layer were extracted from the fitting process. The S parameters and the L_+'s of the 100 and the 500 °C annealed samples were found to be $S(100\,^\circ\text{C}) = 0.5228 \pm 0.0003$, $S(500\,^\circ\text{C}) = 0.5197 \pm 0.0003$, $L_+(100\,^\circ\text{C}) = 14.2 \pm 1.6$ nm, and $L_+(500\,^\circ\text{C}) = 16.1 \pm 2.1$ nm. This implies that the S parameter drops together with the significant decrease in the dislocation-related DLTS signal, while the positron diffusion length does not undergo any significant change.

Carriers can be trapped into the core of a dislocation or into point defects associated with a dislocation. Dislocations are usually negatively charged or neutral in n-type or undoped semiconductor materials and behave normally as weakly bound positron shallow traps.[33] In the cascade trapping model, this type of shallow trap can act as a precursor

for the vacancy-bound positron state.[33] As the positron weakly bound with the dislocation probes a similar electronic environment to the positron bulk state, the positron annihilating from the dislocation shallow trap would have an S parameter that is indistinguishable from the bulk state.[33] However, the presence of dislocation positron shallow traps would be expected to decrease the positron diffusion. In another way, a positron trapped into the vacancy bound to the dislocation would have a higher S parameter as compared to those from the bulk state or from the dislocation shallow trap state. The drop in the S parameter and the invariance of the L_+ after 500 °C thus indicates that the vacancy-type defect concentration decreases and the dislocation concentration does not change. The significant decrease of the dislocation-related DLTS signal at 500 °C annealing can thus be explained if this signal is related to the defect having the structure of the vacancy bound to the dislocation, and the vacancy is annealed, possibly through migration, at 500 °C.

2. Peak at T=350 K in samples with annealing temperatures above 700 °C: Z_1/Z_2 defects

In the 700, 900, and 1400 °C annealed spectra [Fig. 1(b)], a broad signal is clearly shown at the position close to the previously discussed dislocation-related deep-level peak. However, this peak is definitely not the same dislocation-related signal because it does not have the characteristic logarithmic t_p behavior and saturates with $t_p \geqslant 10$ μs, which is a typical behavior for the point defect center. This broad peak is at a position close to the Z_1/Z_2 defects previously found in n-type 6H–SiC samples.[3–5,7,8] Although the DLTS spectra in Fig. 1(b) do not have the appearance of a doublet, we have fitted the peak with two Gaussians to the peak observed in the 1200 °C annealed sample's spectrum. The activation energies and the capture cross sections of the doublet were found to be E_a=0.64/0.75 eV and $\sigma \sim 10^{-16}/10^{-17}$ cm^2, respectively. These activation energies are close to those of Z_1/Z_2 observed in electron-irradiated, proton-irradiated, and He-implanted n-type 6H–SiC samples.[4,5,7,8] The present value of $\sigma \sim 10^{-16}/10^{-17}$ cm^2 is close to that of the Z_1/Z_2 reported in electron-irradiated samples,[5–7] but deviates from that found from proton-irradiated[8] and He-implanted samples[4] ($\sim 10^{-15}$ cm^2). The concentration of Z_1/Z_2 in the present 700 °C annealed He-implanted sample was $(3-8)\times 10^{13}$ cm^{-3}.

Results of previous annealing studies of the Z_1/Z_2 defect have been controversial. The DLTS studies of Zhang *et al.*[2] and Dailbor *et al.*[4] on He-implanted samples have shown Z_1/Z_2 persisting after 1700 °C annealing. In the studies of Gong *et al.*[6] and Aboelfotoh and Doyle,[7] the Z_1/Z_2 defect identified in the 1.7- and the 2-MeV electron-irradiated 6H–SiC annealed at temperatures below 1000 °C.

Comparing the annealing results from different literatures is rather difficult as the discrepancy is possibly due to the differences in the starting SiC material, the sample pretreatment processing, the sample post-treatment processing, etc. In order to eliminate these uncertainties, it would thus be interesting to compare the results obtained in the He-implanted sample to those of the 0.3-MeV electron-irradiated, the 1.7-MeV electron-irradiated, and the neutron-irradiated n-type 6H–SiC samples, in which all the samples were started from the wafers grown under similar conditions. All the contact preparations and annealing were also conducted in the same manner, and all the samples were measured by the same DLTS system. The properties of the Z_1/Z_2 found in the He-implanted, electron-irradiated, and neutron-irradiated samples are summarized in Table I, in which part of the data have already been published in Refs. 12, 13, and 16. From Table I, it is noticed that all the suspected Z_1/Z_2 found in samples irradiated by different particles have values of E_a and σ close to those generally accepted for Z_1/Z_2. However, their annealing behaviors are quite different. The Z_1/Z_2 found in the He-implanted sample anneals after 1600 °C annealing, but those in the 1.7-MeV electron- and neutron-irradiated samples anneal at 900 °C.

TABLE I. Properties of various deep-level defects induced by different kinds of irradiations. All the samples were cut from the starting wafers fabricated under similar environment and undergone the same sample treatment and measurement processes.

	E_a (eV)	$\sigma(E_1)/\sigma(E_2)$ (cm^{-2})	Annealing temperature (°C)
		E_1/E_2	
0.3-MeV electron	0.36/0.44	$\sim 10^{-14}$	1200–1400 °C
1.7-MeV electron	0.37/0.44	$\sim 10^{-14}$	1200–1400 °C
neutron	0.36/0.44	$\sim 10^{-14}$	1200–1400 °C
He[a]	0.38/0.44	$\sim 10^{-14}$	Detectable at 1600 °C
		0.50 eV (E_i)	
0.3-MeV electron	0.50	$\sim 10^{-14}$	300 °C
1.7-MeV electron	0.50	$\sim 10^{-15}$	300 °C
neutron	0.50	$\sim 10^{-15}$	300 °C
He	0.50	$\sim 10^{-15}$	300 °C
		0.53 eV[b]	
He	0.53	$\sim 10^{-15}$	1400 °C
		Z_1/Z_2	
0.3-MeV electron[c]	NA	NA	NA
1.7-MeV electron	0.62/0.72	$\sim 10^{-16}/10^{-17}$	900 °C
neutron	0.62/0.68	$\sim 10^{-16}/10^{-16}$	900 °C
He	0.64/0.75	$\sim 10^{-16}/10^{-17}$	1600 °C

[a]Overlapping with the $E_C-0.31$ eV deep-level defects which anneals at $\sim$1000 °C. E_a and σ were measured from the sample annealed at 1200 °C.
[b]The 0.53-eV defect was only found in the He-implanted samples.
[c]Z_1/Z_2 were not induced with a 0.3-MeV electron irradiation.

It is noticed in Fig. 1(b) that the Z_1/Z_2 signals found in the present 700 and the 900 °C annealed He-implanted samples had similar peak positions, but in the 1200 °C annealed sample the peaks shifted to lower temperatures. The Arrhenius plot of the signal peak in the 700 and the 1200 °C annealed samples' spectra were thus also plotted in Fig. 2 for comparison (assuming the signal as a single peak). From the figure, it is clearly shown that the signals from the two samples annealed at 700 and 1200 °C have different activation energies [E_a(700 °C)=0.65 eV and E_a(1200 °C) =0.74 eV] and capture cross sections [σ(700 °C) $\sim 10^{17}$ cm^2 and σ(1200 °C)$\sim 10^{16}$ cm^2]. The signal observed in the 1200 °C annealed sample thus does not originate from the same exact defect (or defects) as that in the

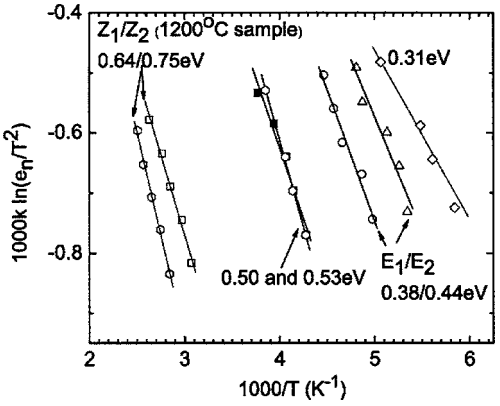

FIG. 4. The Arrhenius plots of the deep-level defects Z_1/Z_2, E_1/E_2, 0.31, 0.50, and 0.53 eV.

700 °C annealed sample. This implies that there is a mechanism occurring in the He-implanted sample, but not in the electron-irradiated samples, which leads to the formation of the new defect (or defects) in the 1200 °C annealed He-implanted sample DLTS spectrum. The microstructure of the new defect and its relation to the original one observed in the 700 °C annealed sample are unknown and thus require further investigations.

B. Peak at $T \sim 250$ K

A DLTS peak was observed at $T \sim 250$ K in the as-He-implanted as well as the 200 °C annealed He-implanted samples [as shown in Fig. 1(a)]. The Arrhenius plot of this signal is shown in Fig. 4. Its energy level, capture cross section, and concentration were found to be $E_C - 0.50$ eV, $\sim 10^{-15}$ cm^2, and $(1-3) \times 10^{14}$ cm^{-3}. This signal anneals out after 300 °C annealing. Similar deep levels at $E_C - 0.50$ eV having similar annealing behaviors were also identified in our 0.3-MeV electron-irradiated, 1.7-MeV electron-irradiated, and neutron-irradiated *n*-type 6H–SiC samples, and the results were shown in Table I. This deep level has activation energy, capture cross section, and annealing behavior very similar to those of the E_i defect previously observed in the electron-irradiated samples.[5]

It is interesting to notice after the annealing out of the $E_C - 0.50$-eV peak slightly lower than 250 K, further annealing of the sample at 700 °C would yield a DLTS peak again with a position slightly higher than 250 K [Fig. 1(b)]. This newly yielded peak finally annealed out again at 1400 °C. From its Arrhenius plot shown in Fig. 4, its activation energy and capture cross section were found to be $E_C - 0.53$ eV and $\sim 10^{-15}$ cm^2, respectively. The activation energy of this newly generated peak is a bit larger than that of the peak at a similar position already annealed out at 300 °C (i.e., the E_i), but their capture cross sections are similar. The thermal stability of this level is more similar to that of RD5 reported by Dalibor *et al.*[4] in their He-implanted samples, although the activation energy of RD5 is a bit smaller [E_a(RD5) $= 0.43-0.47$ eV]. The concentration of the 0.53-eV defect in the 700 °C annealed sample was found to be $(2-3) \times 10^{13}$ cm^{-3}.

C. The E_1/E_2 doublet at $T = 170-240$ K

From Fig. 1, the DLTS signal at $T = 170-240$ K is negligible in the spectrum of the as-He-implanted sample. Its intensity grows with annealing temperature and reaches a maximum at 1200 °C annealing. However, it is worth to point out that the intensity of this signal at its maximum strength (i.e., in the 1200 °C annealed sample) is still smaller than that of the dislocation-related signal found in the as-He-implanted spectrum. Moreover, from the spectrum of the 900, 1200, and 1400 °C annealed samples, it is clear that this signal consists of two peaks and their positions are very close to the previously observed E_1/E_2 defects. The E_1/E_2 concentration of the 1200 °C annealed sample was $(2-5) \times 10^{14}$ cm^{-3}.

E_1/E_2 defects are the dominant deep-level defects created in electron-irradiated 6H–SiC material.[5–7,13] In our previous study,[16] it was clearly demonstrated that in He-implanted and high-energy electron-irradiated (1.7 MeV) 6H–SiC samples, care has to be taken in analyzing the E_1/E_2 signals as the E_1/E_2 peaks merge with another defect signal. This defect has a DLTS peak close to and inseparable from the E_1/E_2 peaks and it vanishes after the 1000 °C annealing. This peak is also the cause of observing different $E_1:E_2$ peak intensity ratio in different samples as the expected value is 1:2. The E_1/E_2 activation energy and capture cross section of the present sample were thus determined from the 1200 °C annealed He-implanted sample. From the Arrhenius plot shown in Fig. 2, the ionization energies and the capture cross sections of the E_1/E_2 defects are found to be $0.38 \pm 0.04/0.44 \pm 0.02$ eV and $(5-9) \times 10^{-14}$ cm^2, which are close to the generally accepted values of E_1/E_2. The E_1/E_2 signals observed in the present He-implanted sample persisted at 1400 °C annealing and even after 1600 °C annealing, E_1/E_2 signals were still visually detectable [see Fig. 1(b)].

It is interesting to compare the properties of the E_1/E_2 found in the present He-implanted sample with those found in the neutron-irradiated and the 0.3-MeV and the 1.7-MeV electron-irradiated samples prepared under similar environments. The results are shown in Table I. It is worth mentioning that for both the 1.7-MeV electron-irradiated and the He-implanted samples, the E_a and the σ values were derived from the data of the 1200 °C annealed samples, because of the existence of the overlapping $E_C - 0.31$-eV defect which annealed at ~ 1000 °C.[16] From Table I, the values of E_a and σ obtained from all the samples coincide with each other. For the neutron-irradiated and the 0.3-MeV and the 1.7-MeV electron-irradiated samples, E_1/E_2 anneals at 1200–1400 °C. This annealing temperature is similar to those of electron-irradiated *n*-type 6H–SiC samples reported by other research groups.[9] However, for our He-implanted sample, the E_1/E_2 signals persist after the 1600 °C annealing and this thermal stability also coincides with that observed in the studies of Zhang *et al.*[2] and Dalibor *et al.*[4] on He-implanted samples.

It is worth investigating the shape of the E_1/E_2 doublet signal found in the spectra of the He-implanted samples annealed at different samples. From Fig. 1(b), the shape of the

doublet significantly changes after the 1200 °C annealing as compared to the 900 °C spectrum. The E_1 peak is stronger than the E_2 peak in the 900 °C annealed spectrum and the $E_1:E_2$ ratio changes to the expected value of ~0.5 after the 1200 °C annealing. This can be explained by the presence of the $E_C-0.31$-eV defect merging with and being inseparable from the E_1, which anneals out after the 1200 °C annealing.[16] Further annealing the He-implanted sample to 1400 °C, which is the annealing temperature of E_1/E_2 induced by electron or neutron irradiations, would not change the shape of the E_1/E_2 doublet in the spectrum, the $E_1:E_2$ ratio, their capture cross sections, nor the activation energies. This implies in the case of the He-implanted samples, that there is no evidence of defect transformation of E_1/E_2 or new defect formation upon the 1400 °C annealing. It is plausible to suggest in the He-implanted samples that the E_1/E_2 signals observed in the 1400 °C annealed sample originate from the same defects as those in the 1200 °C annealed sample. We thus speculate that the superior thermal stability of E_1/E_2 found in the He-implanted *n*-type 6H–SiC samples over those generated by electron irradiation is possibly due to the difference of background defects created by He-implantation and electron irradiation, which interact with the E_1/E_2 centers in different ways upon annealing.

IV. CONCLUSION

We have performed DLTS studies on the He-implanted *n*-type 6H–SiC samples. Defect levels at 0.38/0.44, 0.50, 0.53, and 0.64/0.75 eV below the conduction band and dislocation-related defects have been identified. The microstructure of the dislocation defect was attributed to a vacancy bound to the dislocation. Its intensity significantly dropped after 500 °C annealing, possibly as a result of the migration of the vacancy. The 0.38/0.44- and the 0.64/0.75-eV deep levels had activation energies and capture cross sections close to the previously reported E_1/E_2 and Z_1/Z_2. In the He-implanted samples, the E_1/E_2 center persisted after 1600 °C annealing and the Z_1/Z_2 center annealed at 1400 °C. The thermal stabilities of the E_1/E_2 and the Z_1/Z_2 centers found in the He-implanted samples are more stable than those observed in the neutron- or electron-irradiated samples (annealed at 1400 and 900 °C, respectively).

ACKNOWLEDGMENTS

This work was financially supported by the CERG, RGC, HKSAR under the project no. 7033/05P and the CRCG, HKU.

[1] H. Morkoç, S. Strite, G. B. Gao, M. E. Lin, B. Sverdlov, and M. Burns, J. Appl. Phys. **76**, 1363 (1994).
[2] H. Zhang, G. Pensl, A. Dornen, and S. Leibenzeder, J. Electrochemical Society Extended Abstracts, 89–2, 714 (1989).
[3] G. Pensl and W. J. Choyke, Physica B **185**, 264 (1993).
[4] T. Dalibor, G. Pensl, H. Matsunami, T. Kimoto, W. J. Choyke, A. Schoener, and N. Nordell, Phys. Status Solidi A **162**, 199 (1997).
[5] C. G. Hemmingsson, T. N. Son, O. Kordina, E. Janzén, and J. L. Lindström, J. Appl. Phys. **84**, 704 (1998).
[6] M. Gong, S. Fung, C. D. Beling, and Z. P. You, J. Appl. Phys. **85**, 7604 (1999).
[7] M. O. Aboelfotoh and J. P. Doyle, Phys. Rev. B **59**, 10823 (1999).
[8] A. A. Lebedev, A. I. Veinger, D. V. Davydov, V. V. Kozlovski, N. S. Savkina, and A. M. Strel'chuk, J. Appl. Phys. **88**, 6265 (2000).
[9] A. Kawasuso, F. Redmann, R. Krause-Rehberg, T. Frank, M. Weidner, G. Pensl, P. Sperr, and H. Itoh, J. Appl. Phys. **90**, 3377 (2001).
[10] I. Pintilie, L. Pintilie, and K. Irmscher, Appl. Phys. Lett. **81**, 4841 (2002).
[11] X. D. Chen, C. C. Ling, S. Fung, C. D. Beling, and M. Gong, J. Appl. Phys. **93**, 3117 (2003).
[12] X. D. Chen, S. Fung, C. C. Ling, and C. D. Beling, J. Appl. Phys. **94**, 3004 (2003).
[13] X. D. Chen *et al.*, Phys. Rev. Lett. **92**, 125504 (2004).
[14] Y. Negoro, T. Kimoto, and H. Matsunami, Appl. Phys. Lett. **85**, 1716 (2004).
[15] L. Storasta, J. P. Bergman, E. Janzén, A. Henry, and J. Lu, J. Appl. Phys. **96**, 4909 (2004).
[16] X. D. Chen, C. C. Ling, M. Gong, S. Fung, C. D. Beling, G. Brauer, W. Anwand, and W. Skorupa Appl. Phys. Lett. **86**, 031903 (2005).
[17] M. L. David, G. Alfieri, E. M. Monakhov, A. Hallén, C. Blanchard, B. G. Svensson, and J. F. Barbot, J. Appl. Phys. **95**, 4728 (2004).
[18] A. O. Evwaraye, S. R. Smith, W. C. Mitchel, G. C. Farlow, and M. A. Capano, Mater. Res. Soc. Symp. Proc. **815**, J1.4.1 (2004).
[19] P. Omling, E. R. Weber, L. Montelius, H. Alexander, and J. Michel, Phys. Rev. B **32**, 6571 (1985).
[20] T. Wosinski, J. Appl. Phys. **65**, 1566 (1989).
[21] F. D. Auret, S. A. Goodman, F. K. Koschnick, J.-M. Spaeth, B. Beaumont, and P. Gibart, Appl. Phys. Lett. **73**, 3745 (1998).
[22] N. Sghaier, A. K. Souifi, J. M. Bluet, and G. Guillot, J. Mater. Sci. **12**, 273 (2001).
[23] S. Maximenko, S. Soloviev, D. Cherednichenko, and T. Sudarshan, J. Appl. Phys. **97**, 013533 (2005).
[24] M. Benamara, X. Zhang, M. Skowronski, P. Ruterana, G. Nouet, J. J. Sumakeris, M. J. Paisley, and M. J. O'Loughlin, Appl. Phys. Lett. **86**, 021905 (2005).
[25] W. M. Vetter and M. Dudley, J. Appl. Phys. **96**, 348 (2004).
[26] I. Kamata, H. Tsuchida, T. Jikimoto, and K. Izumi, Jpn. J. Appl. Phys., Part 1 **39**, 6496 (2000).
[27] R. Krause-Rehberg and H. S. Leipner, *Positron Annihilation in Semiconductors* (Springer, Berlin, 1999).
[28] A. van Veen, H. Schut, and P. E. Mijnarends, in *Positron Beams and Its Applications*, edited by P. Coleman (World Scientific, Singapore, 2000), p. 191.
[29] P. J. Schultz and K. G. Lynn, Rev. Mod. Phys. **60**, 701 (1988).
[30] A. Kawasuso, M. Weidner, F. Redmann, T. Frank, P. Sperr, R. Krause-Rehberg, W. Triftshauser, and G. Pensl, Physica B **308**, 660 (2001).
[31] W. Fukarek, R. A. Yankov, W. Anwand, and V. Heera, Nucl. Instrum. Methods Phys. Res. B **142**, 561 (1998).
[32] A. van Veen, H. Schut, J. de Vries, R. A. Hakvoort, and M. R. IJpma, in *Positron Beams for Solids and Surfaces*, edited by P. J. Schultz, G. R. Massoumi and P. J. Simpson, AIP Conf. Proc. No. 218 (AIP, New York, 1990), p. 171.
[33] H. S. Leipner, C. G. Hübner, T. E. M. Staab, M. Haugk, and R. Krause-Rehberg, Phys. Status Solidi A **171**, 377 (1999).